

## Journal Pre-proofs

A novel dissimilar single-lap joint with interfacial stiffness improvement

Armin Yousefi Kanani, Xiaonan Hou, Jianqiao Ye

PII: S0263-8223(20)32667-2

DOI: <https://doi.org/10.1016/j.compstruct.2020.112741>

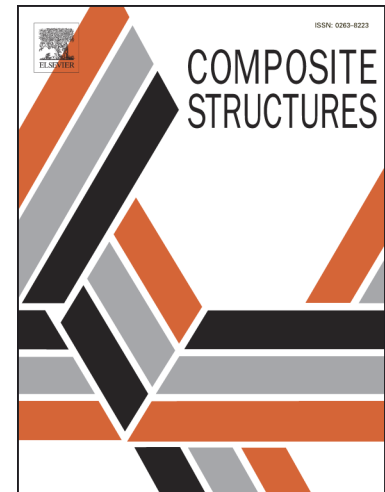
Reference: COST 112741

To appear in: *Composite Structures*

Received Date: 8 June 2020

Revised Date: 7 July 2020

Accepted Date: 26 July 2020



Please cite this article as: Kanani, A.Y., Hou, X., Ye, J., A novel dissimilar single-lap joint with interfacial stiffness improvement, *Composite Structures* (2020), doi: <https://doi.org/10.1016/j.compstruct.2020.112741>

This is a PDF file of an article that has undergone enhancements after acceptance, such as the addition of a cover page and metadata, and formatting for readability, but it is not yet the definitive version of record. This version will undergo additional copyediting, typesetting and review before it is published in its final form, but we are providing this version to give early visibility of the article. Please note that, during the production process, errors may be discovered which could affect the content, and all legal disclaimers that apply to the journal pertain.

© 2020 Elsevier Ltd. All rights reserved.

**A novel dissimilar single-lap joint with interfacial stiffness improvement**

Armin Yousefi Kanani, Xiaonan Hou\*, Jianqiao Ye

<sup>a</sup> Department of Engineering, Engineering Building, Lancaster University, Lancaster, LA1 4YW, UK\* Corresponding author's Email address: [x.hou2@lancaster.ac.uk](mailto:x.hou2@lancaster.ac.uk)**Abstract:**

The increased use of hybrid joints such as bonding composites to metals in aerospace, hull, civil and automotive structures in the past decades makes it essential to find methods to improve the performance of the joints. This study presents both experimental and numerical investigations into a novel dissimilar single-lap joint (SLJ) with interfacial stiffness improvement. The main objective of this research is to minimise the peak stress concentration by reinforcing the lower stiffness adherend's interface through embedding discrete AL patches to increase the performance of the dissimilar single-lap joint with epoxy adhesive. Finite element models (FEA) were developed in Abaqus® software to analyse the effects of thickness and length of the patches, and the failure mechanism due to the reinforcement. Dissimilar single lap joints with different configurations were fabricated and tested using single lap shear tests to validate the numerical analysis. Both the experimental and numerical results show that the strength of the reinforced joint is significantly enhanced by using the aluminium patches.

Keywords: dissimilar single-lap joint, adhesive bonding, interfacial stiffness, FEA

## 1. Introduction

Adhesive bonding is now widely used in multi-material structures due to its advantages over traditional fasteners such as easy manufacturing, more uniform stress distribution and the possibility of joining dissimilar adherends [1]. In the aerospace [2] and the automotive [3] industries, adhesive joints are used to joint several materials that may have different stiffness and strengths. For example, a dissimilar single lap joint (SLJ) connects two different adherends with different mechanical properties, which in practice results in a more complex fracture mechanism and asymmetric stress distribution [4]. Several methods have been suggested by researchers [5]–[7] to optimise the performance of adhesively single lap joints (SLJs). These methods can be categorised into two major groups, i.e., based on material and geometrical modifications. Material modification aims to optimise the stiffness of the adherends/adhesives and geometrical modification attempts to change the shape of the adherends/adhesives.

Sawa et al. [8] demonstrated a method for analysing the stress distribution in SLJs of dissimilar adherends (aluminium (AL)/mild steel) under tensile loads. Moreover, they also numerically studied the effects of Young's modulus, thickness and length ratios between the adherends, and the ratio of the adhesive thickness to the adherends on the stress distributions. Their results show that the stress singularity increases at the free edge of the interface in the adherend with lower stiffness. Vinson [9] found that increasing the flexural and extensional stiffness of the adherends could minimise the maximum peel and shear stresses at the overlap edges. Reis et al. [4] used three different adherends (laminated composite, high elastic limit steel, and the 6082-T6 aluminium alloy) to study the effect of adherends' stiffness on the shear strength of single-lap adhesive joints. Their research concludes that the effect of the over-lap length on the shear strength depends on the stiffness of the adherends. Ruadwska [10] analysed the tensile strength of bonded joints of similar and dissimilar material by considering both experimental and **cohesive zone model (CZM)** approaches for fracture predictions. Pinto et al. [11] evaluated the tensile strength of SLJs of similar and dissimilar adherends bonded with an acrylic adhesive by using **CZM** simulations. Their numerical results demonstrate that an increase of adherends' stiffness will reduce bending of joints, which leads to a lower stress concentration at the edges, and, consequently, improves the strength of the joints.

Z-axis penetrative reinforcement is a new and commonly used [12]–[19] hybrid joining approach that shows an improvement of joint strength. Isalm et al. [15] investigated the effects of through-thickness pinning reinforcement on the strength and the damage tolerance of hybrid steel–composite SLJs. The results showed that the SLJs with reinforcement pins experienced an increase in the joint strength up to 58% depending on the number and location of the pins. Rezvaninasab et al. [16] utilised pins and wires as reinforcing elements to improve the strength of SLJs under tensile and bending loading conditions. Matsuzaki et al. [17] used a bolted co-cured hybrid joining approach to improve the strength of glass **fibre reinforced polymer (GRP)** aluminium co-cured lap joints. Their experimental results show that the bolted/co-cured hybrid joints have 1.84 times higher maximum shear strength in comparison with

that of only co-cured hybrid joints. In another work, Matsuzaki et al. [18] used inter-adherend (IA) fibre that penetrated the composite and holes in the metal adherend to reinforce polymer co-cured composites. They concluded that the IA fibre performed as a bridge between the AL and the composite adherend, which efficiently arrested crack propagation. Because of this, the joint strength increased significantly compared to the SLJs without IA fibres. Fawcett et al. [19] conducted research in using cold worked penetrative reinforcements to enhance joining between AL and GRP. Their static tensile test results indicate that the new reinforcement method enhances the maximum failure load and the displacement before failure.

Another hybrid joining method showing positive results is the use of multi-layers' reinforcement, which relies on the local reinforcement of the composite laminate with high-strength metal layers. Santos et al. [20] investigated the advantage of strengthening carbon fibre reinforced polymers (CFRP) with metal laminate by using adhesive layers in the interfaces between titanium and composite with different lay-up configurations. Morgado et al. [21] analysed the influence of using metal laminates as the reinforcement in SLJs under tensile and impact loading conditions. Their study showed that the reinforcement method could increase the joint strength, energy absorption, and eliminate delamination between composite layers. Camanho et al. [22] introduced a novel metallic insert with tapered ends to increase the efficiency of bolted composite single-lap joints. The experimental results show that the metallic insert provides new pathways for load transfer, which leads to higher maximum load and joint efficiency.

Single-lap joints (SLJ) are utilised in many engineering applications due to their lower cost and simplicity. However, there are few works available in the literature that focus on the optimisation of dissimilar SLJs for improving performance. The main objective of this research is to improve the performance of dissimilar single-lap joints between aluminium (AL) and Polyphthalamide (PPA). In order to do this, a novel design is introduced for dissimilar SLJs by reinforcing the interface of the lower stiffness adherend (PPA) using AL patches of different dimensions. First, numerical analyses are carried out to assess the effect of dimensions (thickness and length) of the AL patches on the performance of the joints. Then, the strength and failure mechanism of the dissimilar SLJs are discussed. Finally, experiments are conducted for each modified dissimilar SLJs to verify the strength improvement of each modification.

## 2. Experiment

### 2.1 Material selection

In this study, the adherends are cut from aluminium alloy 6082 T6 bar and Polyphthalamide (PPA) plates. The PPA is commercially called Grivory HTV-5H1 black 9205, a reinforced engineering thermoplastic made of 50% glass fibre, based on a semi-crystalline, partially-aromatic polyamide. In addition, the epoxy adhesive used for this work was Loctite EA 9497, a two-component material of medium viscosity which cures at room temperature. The material properties of the adherends and adhesives were characterised through tensile tests based on ISO EN 485-2:2004 standard for adherends and ISO 527-2 for brittle adhesive from our previous work (Table 1). The metal reinforcement patches are made of aluminium, which is provided in plate form with various thickness.

Table 1: The bulk property of adherends, adhesive, and metal patches [23]

Property	Aluminium 6082 T6	Polyphthalamide (PPA)	Loctite EA 9497
Young Modulus (MPa)	70770 ± 380	17620 ± 600	7705.35 ± 468
Yield Stress (MPa)	254.59 ± 3.20	241.33 ± 10.4	46.29 ± 3.13
Elongation at fracture (%)	10.83 ± 0.95	1.71 ± 0.04	0.71 ± 0.09
Poisson Ratio	0.30 ± 0.01	0.32 ± 0.04	0.29 <sup>a</sup>
Density (tonne/m <sup>3</sup> )	2.7 <sup>a</sup>	1.65 <sup>a</sup>	1.1 <sup>a</sup>

<sup>a</sup>Manufacturer data

### 2.2 Joint configuration, fabrication and testing

In this study, two types of single-lap joints are manufactured (Figure 1), which are the un-modified joint (type-0), and the joint with two aluminium patches on the PPA's interface along the bonding area (type-1). The conventional single-lap joint (type-0) is used as a benchmark design.

Type 1 specimens are categorised into two groups to analyse the effects of dimensions of the patches. In category A, the thickness of the patches varies with a constant length. In category B, the length of the patches varies with a constant thickness.

All SLJs are made with the same value of grip-grip separation points ( $L_t = 125$  mm), the thickness of the adherend ( $t_s = 3$  mm), the thickness of the adhesive ( $t_A = 0.2$  mm), the width of the adherend ( $w = 25$  mm) and the overlap length of bonding ( $L_{AD} = 25$  mm). The thickness of the adhesive used in the bond-line (E-F and G-H) between the AL patches and the PPA is  $t_{A1} = 0.2$  mm. Tabs with a dimension of  $L_{TAB} = 25$  mm are bonded at the end of the joints to secure correct alignment in the testing machine.

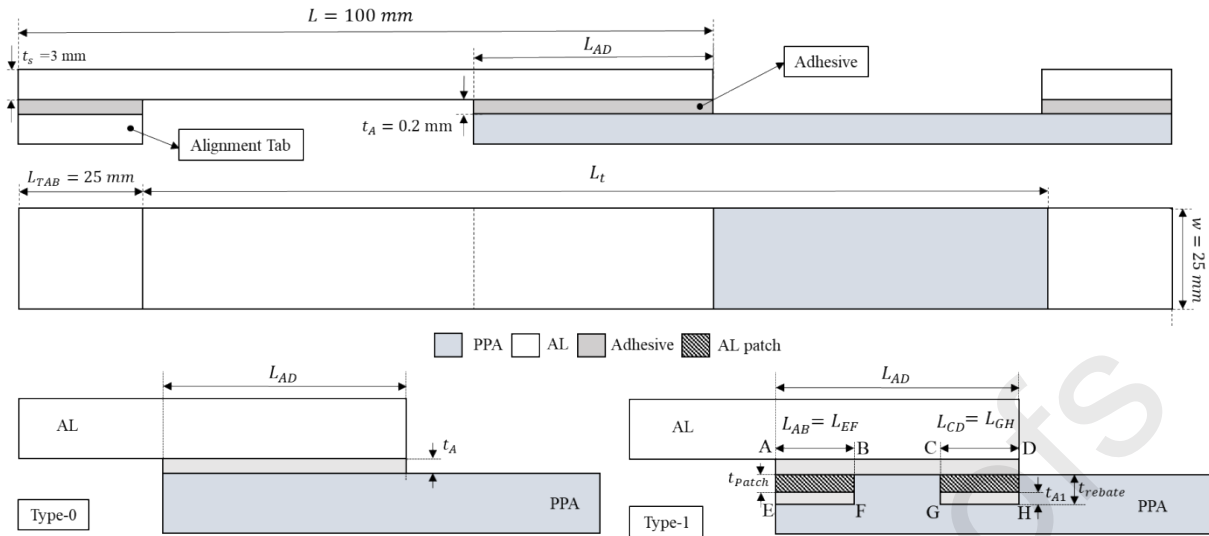


Figure 1: Dimensions and geometry of unmodified and modified dissimilar SLJs

The manufacturing process begins by cutting the aluminium and the PPA plates into the desired dimension ( $L = 100 \text{ mm}$ ). The CNC machine is used to create rebates at the bonding area of the PPA adherend based on their design categories (Table 2) to provide space for the AL patches (Figure 2). In category A (Model I-IV), the length of the patches are fixed ( $L_{EF}$  and  $L_{GH} = 5 \text{ mm}$ ) and the thickness of the AL patches ( $t_{patch}$ ) changes. The thickness of the rebates is equal to the thickness of the AL patches plus the thickness of the adhesive ( $t_{rebate} = t_{patch} + t_{A1}$ ). In category B (Model-II and Model V-VII), the length of the AL patches ( $L_{EF}$  and  $L_{GH}$ ) changes, whilst the thickness of the AL patches is fixed by selecting the optimal thickness from category A based on the stress analysis results.

Table 2: The configuration of the SLJ with various AL patches thickness on the bonding surface

Category	ID	Type	$t_{patch}$ (mm)	$L_{EF}$ and $L_{GH}$ (mm)
--	<b>Model-0</b>	0	--	--
A	<b>Model-I</b>	1	0.2	5
	<b>Model-II</b>	1	0.4	5
	<b>Model-III</b>	1	0.6	5
	<b>Model-IV</b>	1	0.8	5
B	<b>Model-II</b>	1	0.4	5
	<b>Model-V</b>	1	0.4	7.5
	<b>Model-VI</b>	1	0.4	10
	<b>Model-VII</b>	1	0.4	12.5

The same surface treatment is carried out for all SLJs to increase the bonding strength. Firstly, the bonding surfaces are prepared with grit blasting (Guyson Grade 12-Metallic Blast Media, corresponded to particles size of 150-250 microns) and then cleaned with compressed air to remove any extra dust created during the blasting process, before being subsequently cleaned with Acetone and Loctite SF 706. The curing process is carried out at room temperature in two steps. First, the AL patches are bonded to the PPA interface by applying pressure with spring clamps for 24 hours (Figure 2-3). Then, the aluminium adherend is bonded to the modified PPA by using the same method and left at the room temperature for seven days to reach fully cured strength. Wire spacers, with a diameter of 0.2 mm, are

used to control the bond-line thickness, and the excess adhesives are removed at the overlap edges to provide identical conditions for all specimens.

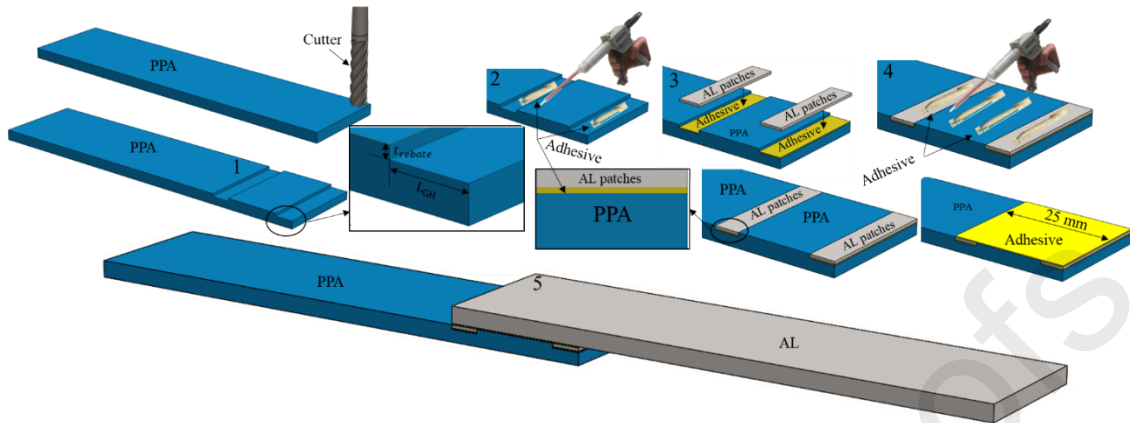


Figure 2: The manufacturing process of the modified SLJ with AL patches

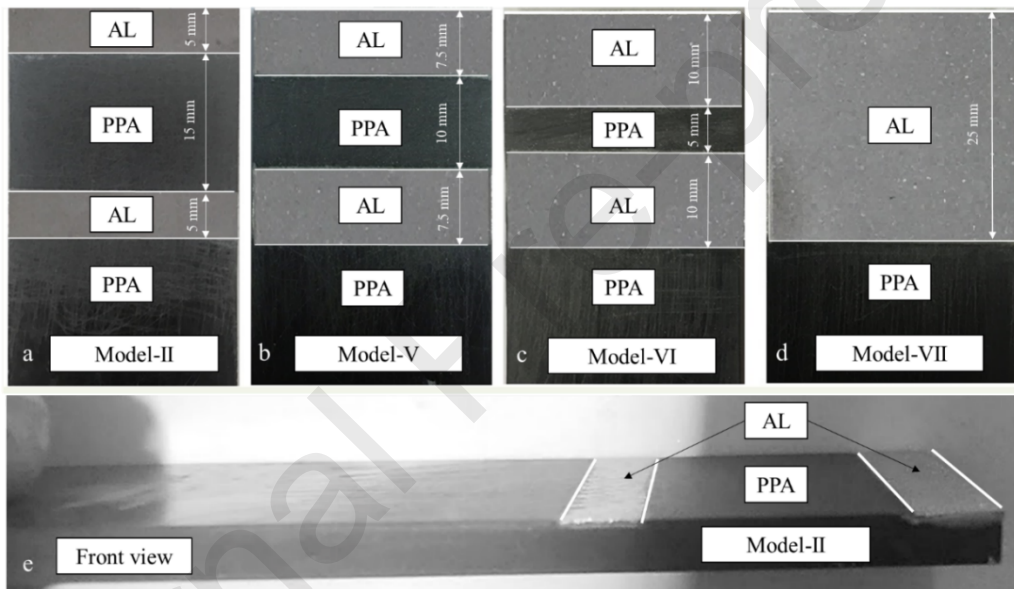


Figure 3: The PPA adherends with AL patches, top view of (a) Model-II, (b) Model-V, (c) Model-VI and (d) Model-VII and (e) the front view of the Model-II

All specimens are tested under tensile loading on an Instron 3380 series machine with 100 kN load cell at the room temperature. The loading rate is controlled by a displacement of 0.5 mm/min. A high-resolution camera is used to observe the failure process of the joints (Figure 4).

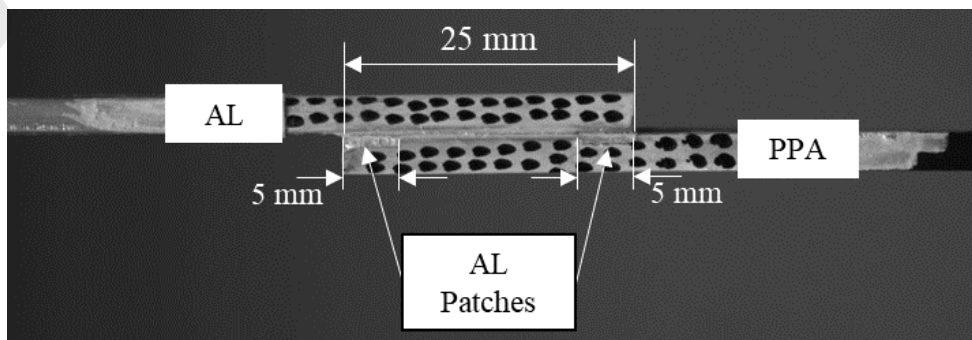


Figure 4: Modified single-lap joint with AL patches

### 3. Finite element model

Two-dimensional (2D) nonlinear numerical models of the modified and unmodified single-lap joints are developed in Abaqus® for the analyses of stress distribution, failure mechanism and joint strength. 2D (plane strain) model provides a reasonable simplification of the 3D model for the bonded joint [24]. The first aim of the finite element analysis (FEA) is to obtain the optimum dimensions (thickness and length) of the AL patches along the bond-line for dissimilar single-lap joints.

The explicit nonlinear analyses are used to simulate the fast crack growth along the bond-line for the epoxy adhesive. Two different cases are analysed. Case-1 utilises a CZM to predict the strength of the joint and Case-2 is used only for stress analysis along the bond-line without considering damage (CZM properties) to find the ideal size of the AL patches.

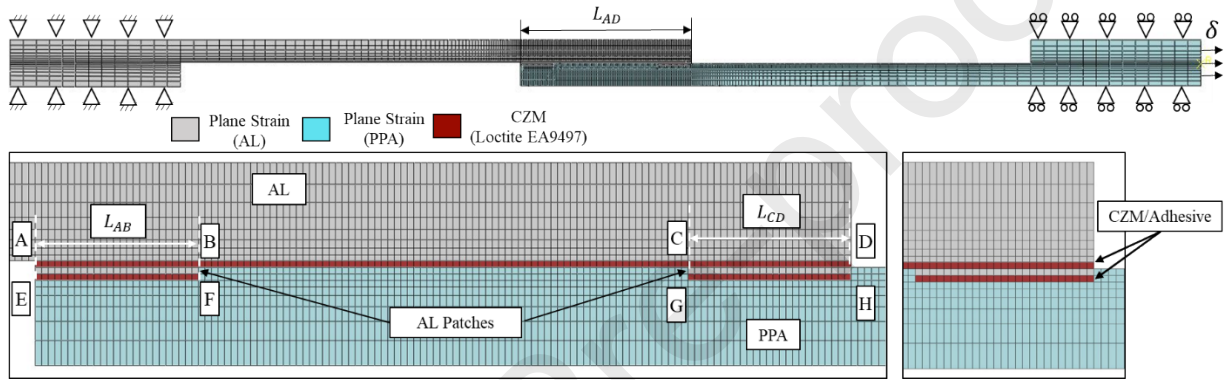


Figure 5: Case-1 mesh details of modified (Model-I) SLJ

In Case-1, both adherends are meshed with plane-strain elements (CPE4R in ABAQUS) by using the single-bias method in the thickness direction with a minimum and maximum element size of 0.2 mm and 0.8 mm, respectively. Mesh size of 0.2 mm along the length is chosen for the over-lap area according to the convergence study, and the single-bias effect is used in other parts of the adherends with a minimum element size of 0.2 mm and a maximum element size of 2 mm to reduce computation time. In addition, the AL patches are meshed with 4-noded plane-strain elements of 0.2 mm  $\times$  0.2 mm. The bulk material properties from Table 1 are utilised for the adherends and the AL patches.

The adhesive sections (A-D, E-F and G-H) are modelled with one layer of CZM elements (COH2D4) with a thickness of 0.2 mm (Figure 5). The CZM elements specify the interface properties between the adherend and the adhesive, which include elasticity, plasticity and susceptibility to damage.

Table 3: CZM parameters for Loctite EA 9497 [23]

Property	Loctite EA 9497
$G_{Ic}$ (N/mm)	$0.26 \pm 0.06$
$G_{IIc}$ (N/mm)	$0.90 \pm 0.38$
$t_n$ (MPa)	$25.35 \pm 10.26$
$t_s$ (MPa)	$16 \pm 5$

Table 3 presents the CZM parameters obtained in previous research from single-mode coupon tests. The nominal traction stress consists of two components, i.e., in normal ( $t_n$ ) and shear ( $t_s$ ) directions,

that allows simulating damage initiation in the bond-line. The  $G_{IC}$  and  $G_{IIC}$  are fracture energy and represent the areas under the traction separation law graphs in the normal and shear directions, respectively [25].

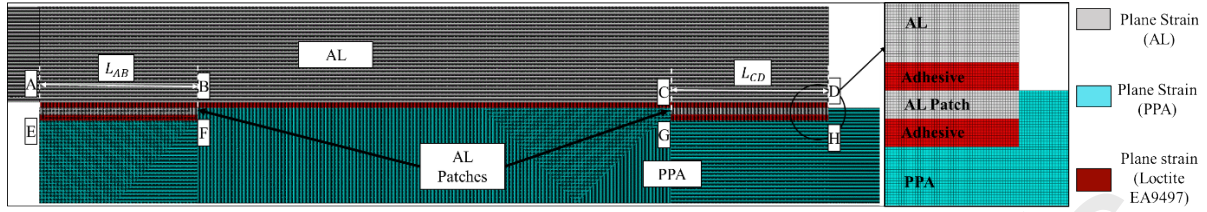


Figure 6: Case-2 mesh details of modified (Model-I) SLJ

As shown in Figure 6, a refined mesh is utilised for Case-2 to capture a more detailed stress gradient at the overlap edges [26]. The adhesive sections are meshed with plane strain element (CPE4R) with a thickness of 0.02 mm along the length and through-thickness. The adherends are meshed with 0.02 mm along the bond-line, and a single-bias method is used in other parts of adherends with minimum and maximum elements size of 0.02 and 0.2 mm, respectively.

## 4. Results and Discussion

### 4.1 Stress analysis

This section aims to find the effects of the length and thickness of the AL patches, located in the bonding area, on the stress distributions of the dissimilar single-lap joints (SLJs). This is carried out by utilising the FE model in Abaqus® software to simulate a set of SLJs (shown in Table 2) with various AL patches configurations to find the optimum one. The main objective of the proposed design is to reduce stress concentration at the overlap edges, caused by asymmetric stress distribution in the dissimilar SLJs. This can be more beneficial for epoxy adhesive, compared with the flexible and ductile adhesives, as the bond-line edges play a significant role in carrying the external load [27]. Thereby, the epoxy adhesive is selected for this study.

The conventional SLJ (Model-0) is used in this section as a reference model for comparisons. All the figures show elastic stresses in the middle of the adhesive layer when the applied axial displacement is 0.01 mm. Peel and shear stresses are normalised ( $\sigma_y/\tau_{avg}$  and  $\tau_{xy}/\tau_{avg}$ , respectively) by the average value of the shear stress ( $\tau_{avg}$ ) along the bond-line for each design. The position along the bond-line ( $x$ ) is also normalised by the total overlap length ( $L_{AD}$ ). The overlap length is divided into three sections based on the trend of the stress distribution. Section I and Section III represent the peak stress concentration zones at the free edges of the aluminium and the PPA, respectively, and Section II shows stress at the overlapping inner region.

#### 4.1.1 The effect of the AL patch thickness

Four different models (Model-I, Model-II, Model-III and Model-IV) are used to study the effect of the thickness of AL patches by keeping the length ( $L_{EF}$  and  $L_{GH} = 5$  mm) constant and varying thickness ( $t_{patch} = 0.2$  mm, 0.4 mm, 0.6 mm and 0.8 mm).

As it is clear from Figure 7, both the peel and shear stresses are more uniform at the mid-section (Section II) of the adhesive with higher peak stresses at the edges (Section I and III), which are caused, respectively, by the rotation of the adherends [28] and the material discontinuity of the adherends at the free edges [29]. Moreover, the asymmetric stress distribution is evident, which is due to the stiffness mismatch of the adherands.

The conventional dissimilar SLJ without any modification (model-0) has a higher peak value of  $\tau_{xy}/\tau_{avg}$  in Section III (10.8) compared with the value in Section I (4.88). This suggests that in a dissimilar joint, the adherend with lower stiffness is more influential to the strength of the entire joint [4]. On the other hand, the  $\sigma_y/\tau_{avg}$  shows lower peak values in Section-III due to increased longitudinal deformation of the PPA adherend [11].

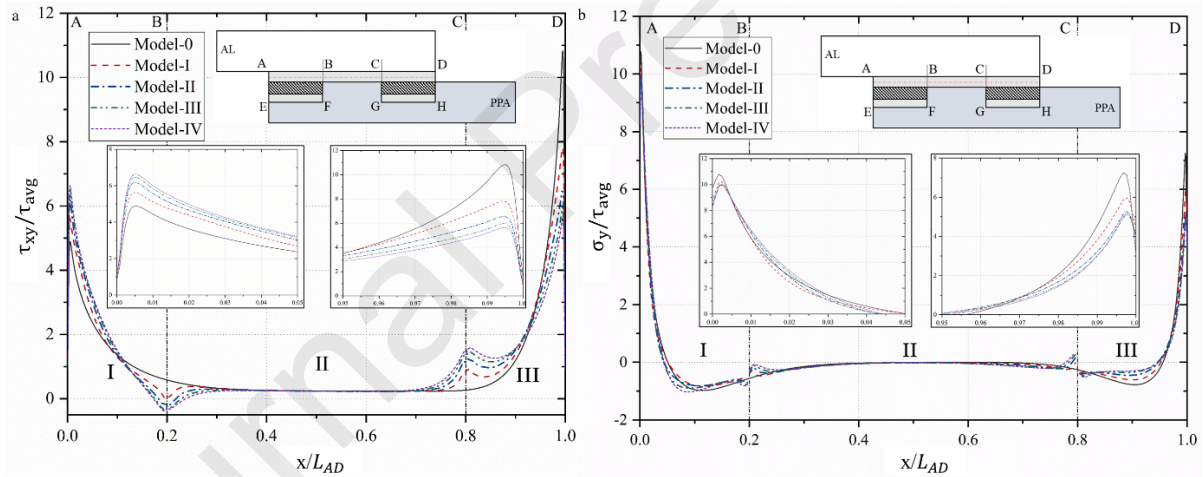


Figure 7: The comparison of normalised shear  $\tau_{xy}$  peel  $\sigma_y$  stresses along the adhesive mid-thickness (A-D)

In Section III, the peak value of  $\tau_{xy}/\tau_{avg}$  at the edges of the SLJs with AL patches (Model-I, Model-II, Model-III and Model-IV) are significantly lower than that of the unmodified SLJ (Model-0). This can be explained by the improved local interface stiffness in the PPA adherend with AL patches, which leads to higher global rigidity of the joint.

Table 4 shows the percentage difference of stresses at two edges with respect to Section-I. The difference between the peak value of the  $\tau_{xy}/\tau_{avg}$  reduces significantly in the modified SLJs in comparison to the conventional dissimilar SLJ. Model-II ( $t_{patch}=0.4$ ) has the least difference between the peak  $\tau_{xy}/\tau_{avg}$  values (5.49%) at both edges among all other models, which results in a more symmetrical distribution of the shear stress.

The peak value of the  $\sigma_y/\tau_{avg}$  is significantly lower in Section III of the modified SLJs than that of the unmodified SLJ. The peak  $\sigma_y/\tau_{avg}$  is only slightly lower in Section I. This leads to a higher difference between the peak  $\sigma_y/\tau_{avg}$  values at both edges (Section I and III) for the modified dissimilar SLJs in comparison to the unmodified dissimilar SLJ.

The difference between peak  $\tau_{xy}/\tau_{avg}$  at Sections I and III decreases from 121.72% in Model-0 to 38.72% in Model-I, while the difference of the peak  $\sigma_y/\tau_{avg}$  values at both edges increase from 32.36% in Model-0 to 41.54% in Model-I. It can be concluded that the reduction of the unsymmetrical shear stress distribution of the dissimilar single lap joint leads to the more significant unsymmetrical behaviour of the peel stress.

By increasing the thickness of the AL patches from 0.4 mm (Model-II) to 0.8 mm (Model-IV), the difference of the peak  $\tau_{xy}/\tau_{avg}$  values increases gradually from 5.49 % in Model-II to 15.23% in Model-IV, while the difference of the peak  $\sigma_y/\tau_{avg}$  at both edges reduces slightly from 49.47% in Model-II to 48.54% in Model-IV. This suggests that the proposed design has a more significant effect on the shear stress distribution than on the peel stress for the joints with thicker patches.

Table 4: The maximum  $\tau_{xy}/\tau_{avg}$  and  $\sigma_y/\tau_{avg}$  at the corners of the bond-line (A-D)

ID	Section-I	Section III	Difference (%)	Section-I	Section-III	Difference (%)
	$\tau_{xy}/\tau_{avg}$	$\tau_{xy}/\tau_{avg}$		$\sigma_y/\tau_{avg}$	$\sigma_y/\tau_{avg}$	
<b>Model-0</b>	4.88	10.82	121.72	10.76	7.25	32.36
<b>Model-I</b>	5.63	7.81	38.72	10.23	5.98	41.54
<b>Model-II</b>	6.19	6.53	5.49	10.45	5.29	49.37
<b>Model-III</b>	6.52	5.99	8.12	10.06	5.15	48.80
<b>Model-IV</b>	6.63	5.62	15.23	9.99	5.14	48.54

In the mid-section of the bond-line, Model-0 has the smoothest normalised peel and shear stress distributions, while the peak values of  $\tau_{xy}/\tau_{avg}$  and  $\sigma_y/\tau_{avg}$  increase gradually with the increase of the thickness of the AL patches. The comparisons of Model-0 and Model-IV show that the peak values of the stresses at Section-II increase from -0.07 in Model-0 to -1.0 in Model-IV for  $\sigma_y/\tau_{avg}$  and from 0.48 in Model-0 to 1.42 in Model-IV for  $\tau_{xy}/\tau_{avg}$ , respectively. This can be justified by the sudden change in the stiffness of the bonding interface of the PPA adherends.

Figure 8 shows the stress plots at the mid-section of the adhesive layers (E-F and G-H) for various thickness of the AL patches. Break lines are used in the X-direction (over-lap) to provide a better comparison. In Model-IV, the peak  $\tau_{xy}/\tau_{avg}$  values at the outer edge (E) of the adhesive layer (E-F) at Section-I is almost doubled in comparison to that of Model-I, while in contrast the peak  $\tau_{xy}/\tau_{avg}$  value remains unchanged at the outer edge (H) of the adhesive layer (G-H) at Section-III. However, the peak

$\tau_{xy}/\tau_{avg}$  values increase significantly in both inner edges (F and G) of the bond-lines EF and GH when the thickness of the AL patches increase from 0.2 mm (Model-I) to 0.8 mm (Model-IV).

The peak value of the  $\sigma_y/\tau_{avg}$  does not change noticeably at both edges when the thickness of the AL patches increases from 0.2 mm (Model-I) to 0.6 mm (Model-III). On the other hand, Model-IV experiences a slight increase in the peak  $\sigma_y/\tau_{avg}$  by 12.5% at Section-I and 15.75% at Section-III, respectively, in comparison to Model-III.

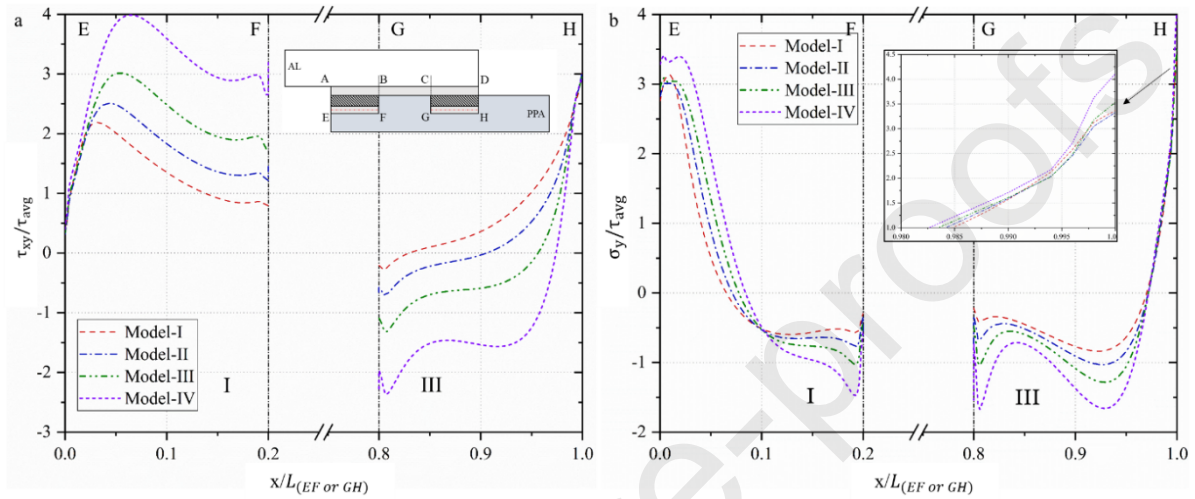


Figure 8: The normalised (a) shear and (b) peel stress plots at the mid-section of the adhesive layer (E-F and G-H)

It can be concluded that the AL patch with a thickness of 0.4 mm (Model-II) provides more symmetric shear stress distribution along bond-line (A-D) in comparison to other models. In addition, the peak value of the stresses at the adhesive layer of EF and GH in Model-II is lower than that in Model-III and Model-IV. Therefore, a thickness of 0.4 is selected as the best thickness of the AL patches.

#### 4.1.2 The effect of the length of the AL patch

Four different models (Model-II, Model-V, Model-VI and Model-VII) are used to study the effect of the length of AL patches by keeping the thickness ( $t_{patch} = 0.4$  mm) constant and varying the length of patches ( $L_{EF}$  and  $L_{GH} = 5$  mm, 7.5 mm, 10 mm and 12.5 mm).

Figure 9 shows the comparison of the normalised shear ( $\tau_{xy}/\tau_{avg}$ ) and peel ( $\sigma_y/\tau_{avg}$ ) stresses distributions for various lengths of the AL patches. It is clear that changing the length of the AL patch does not change the peak stress values at the bond-line (A-D) edges. In Section-II, Model-VII has the smoothest peel and shear stress distributions in comparison to other modified models, as the AL patch covers the full length of the overlap and there is not any sudden change in the interface stiffness of the adherend along the bond-line (A-D).

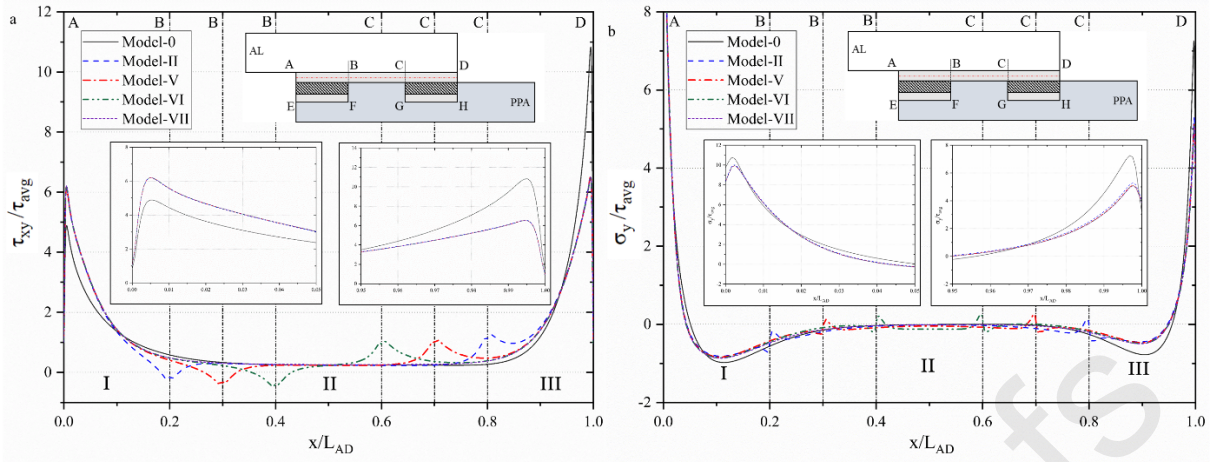


Figure 9: The comparison of the normalised shear  $\tau_{xy}$  and peel  $\sigma_y$  stresses at the adhesive mid-thickness (A-D)

Figure 10 shows the stress plots at the mid-section of the adhesives layers (E-F and G-H) with the different length of the AL patches. In Sections-I and III, it is clear that the peak stresses at the edges increase with the increase of the length of the patches.

The comparison of Model-II and Model-VII shows that the peak value of the  $\tau_{xy}/\tau_{avg}$  increases at Section-I from 2.48 in Model-II to 4.20 in Model-VII, which represents an increase of 69.35 %. The same trend is observed at Section-III with a 71.66% increase in the peak  $\tau_{xy}/\tau_{avg}$  value of Model-VII in comparison to Model-II. This can be justified by the increasing effect of the bending moment due to the longer patches, which results in higher stress concentration at the edges. The peak value of  $\sigma_y/\tau_{avg}$  follows the same tendency and increases in Model-IV by 63.33 % and 61.72 % at Section-I and Section-III, respectively in comparison to Model-II.

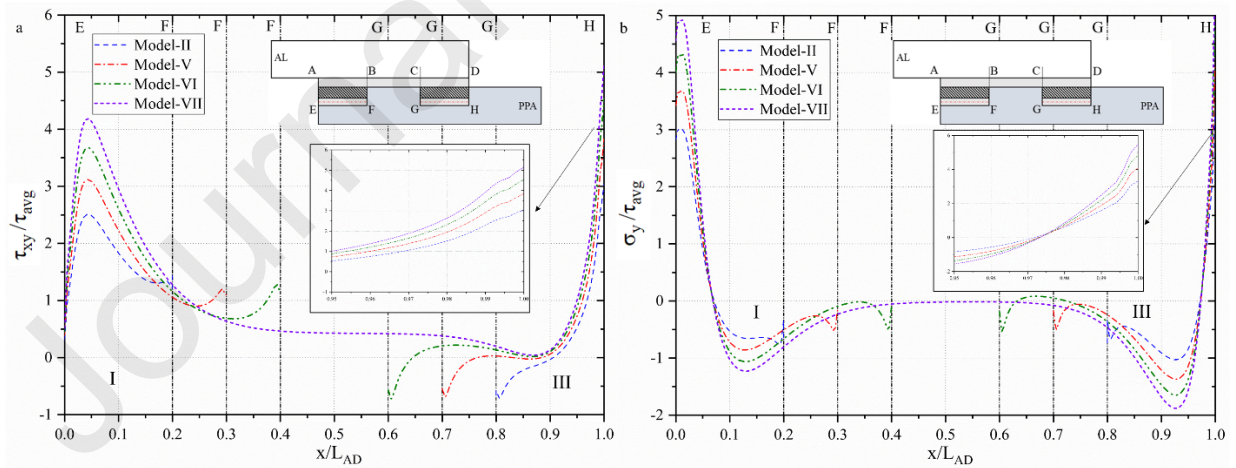


Figure 10: the normalised (a) shear and (b) peel stress plots at the mid-section of the adhesive layer (E-F and G-H)

It can be concluded that embedding discrete AL patches can significantly decrease peak peel and shear stresses at the bond-line. Model-II has the best configuration by providing lower stress concentration at the over-lap edges for all layers of the adhesives (A-D, E-F and G-H).

## 4.2 Joint Strength

In this section, the effect of thickness and length of the AL patches on the strength of the dissimilar SLJs are studied experimentally and numerically. The average joint strength (**failure load over the bonding areas**) is obtained experimentally from four specimen tests, and the numerically predicted strength is obtained using the CZM method. Figure 11 presents the comparisons between the experimental and numerical strength of different configurations of the SLJs (Shown in Table 2).

As seen in Figure 11, there is a good agreement on the average joint strength between the numerical and experimental results. The average joint strength of the dissimilar SLJs increases significantly by adding AL patches to the bond-line. The joint strength increases from 3.86 MPa in Model-0 to 7.25 MPa in Model-I, which corresponds to an 87.82% improvement. This can be explained by the increase of overall stiffness of the novel dissimilar SLJs, which leads to smaller bending moment and stress concentration, as previously discussed in Section 4.1.1.

By increasing the thickness of the AL patches from 0.2 mm to 0.4 mm, the tested joint strength increases by only 0.96% to 7.32 MPa for Model-II in comparison to Model-I. On the other hand, the numerically predicted strength of Model-II is 7.73 MPa, which is 8.11% higher when compared to Model-I (7.15 MPa). The slightly higher joint strength from the numerical model in comparison to the experimental result can be justified by the significant stress improvement at the edges of the bond-line (A-D) for Model-II in comparison to Model-I.

The tested joint strength decreases significantly by 12.43% to 6.41 MPa when the AL patch thickness increases from 0.4 mm (Model-II) to 0.6 mm (Model-III), as it was expected from the stress analysis results. The numerical results for Model-III follows the same trend with a slightly lower reduction in joint strength (6.63%) compared to Model-II.

The joint strength from the numerical simulation shows further reduction by increasing the thickness of the AL patches to 0.8 mm (Model-IV). This reflects the findings in Section 4.1.1, where a higher stress concentration at the edges of the adhesive layers (E-F and G-H) are obtained for Model-III and Model-IV due to thicker rebates. This suggests that increasing the thickness of the AL patches to achieve a higher failure load for the proposed dissimilar bonded joint is only effective within a limited range.

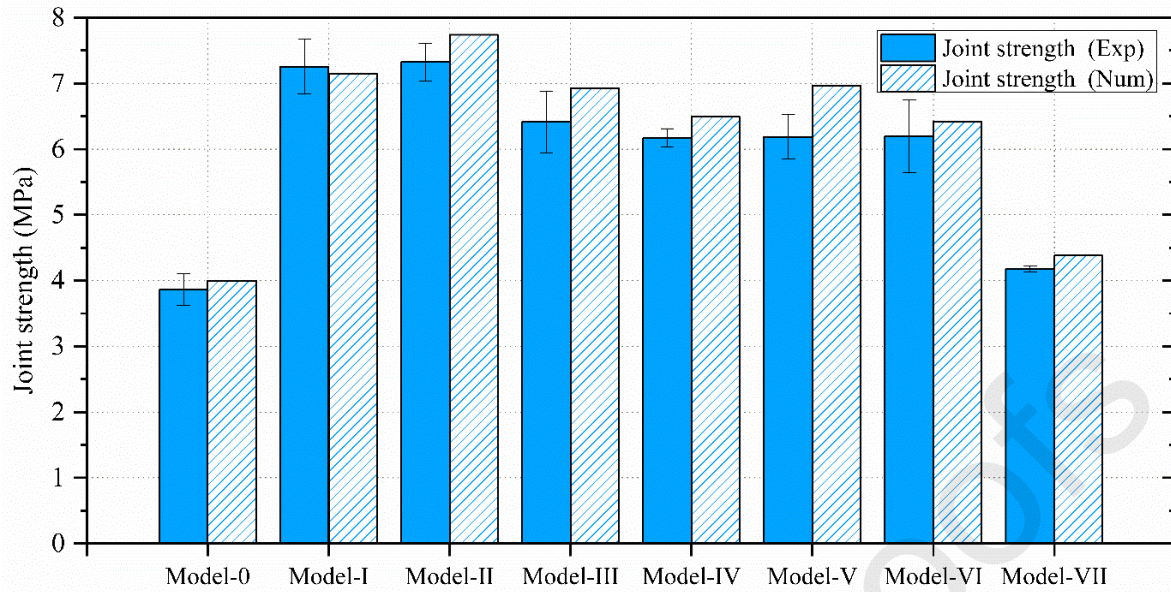


Figure 11: Comparison between the experimental and numerical strengths of the various dissimilar joints

Model-II, Model-V, Model-VI and Model-VII in category B, which have the same thickness ( $t_{\text{patch}} = 0.4$  mm), are compared with each other to analyse the effect of the length of the AL patches. The experimental results show that by increasing the length of the AL patches from 5 mm (Model-II) to 7.5 mm (Model-V), the average joint strength decreases considerably from 7.32 MPa in Model-II to 6.18 MPa in Model-V, which corresponds to a 15.57% reduction. The same trend is followed by the numerical results with a smaller reduction (6.1%) of the joint strength. This can be justified by the higher value of the peel and shear stresses at the edges for longer AL patches (shown in Section 4.1.2), adversely affecting the epoxy adhesive layers (E-F and G-H), which is sensitive to the peak stresses at the edges.

Although the numerical results predicted a further reduction of the joint strength by 7.75% when the length of the AL patches increases from 7.5 mm (Model-V) to 10 mm (Model-VI), the experimental results do not show a noticeable difference in the joint strength. However, when the AL patch covers the total length of the bond-line in Model-VII, the average joint strength is decreased by 43.57% experimentally and 43.33% numerically when compared to model-II. The joint strength of Model-VII is higher only by 7.43% compared to the conventional dissimilar SLJ (Model-0). This suggests that the worst performance of the proposed dissimilar bonded joint occurs when the AL patches are replaced by a single one across the length of the overlap.

It can be concluded from the experimental results that the proposed novel design can enhance the strength of the dissimilar SLJ as much as 90.67% (Model-II). This novel design for dissimilar SLJ has superior advantages over available designs in the literature such as notches (38.33% improvement in Ref [30]), spew fillet (36.3% improvement [31]), bi-adhesive (41% and 50% improvement in Ref [30] and [32], respectively) and surface treatment (Improvement of 46.87% in Ref [33], 35% in Ref [34] and 32% in Ref [35]).

### 4.3 Damage variable analysis

This section presents the overall scalar stiffness degradation (SDEG) [36] of the CZM elements along the bond-lines (A-D, E-F and G-H) to understand the failure process of the proposed dissimilar SLJs. The damage variable (SDEG) varies between 0 (undamaged) and 1 (fully damaged). Figures 12 and 13 show the SDEG plots for various lengths and thicknesses of the AL patches under maximum failure load.

As can be seen from Figure 12(a), the SDEG plot shows asymmetric behaviour for Model-0 with a larger area of the bond-line (A-D) under damage toward the PPA side (22.32%) compared to the AL side (13.30%). This can be explained by the differences in the stiffness of the adherends, which leads to a higher stress concentration toward the lower stiffness adherend (PPA). Moreover, the phenomenon suggests that cracks are initiated at the PPA side due to the sensitivity of the epoxy adhesive to the high peak stresses at the edges.

The total area of damage along the over-lap length (A-D) increases from 35.62% in Model-0 to 40.69% in Model-I (Figure 12(a)). The damage shifted slightly from the right corner (D) to the inner section (C) of the bond-line (A-D) with a slightly smaller value of the SDEG compared to the bond-line (G-H) (Figure 12(b)). The unsymmetrical stiffness degradation is also observed in the bond-lines (E-F and G-H), with higher SDEG value and the larger area of the overlap under damage in bond-line (G-H) compared to bond-line (E-F). This suggests that in the modified SLJs, the crack is initiated at the bond-line (G-H) then propagates to the inner section of bond-line (A-D), which is also observed experimentally (Figure 14).

By increasing the thickness of the AL patches from 0.2 mm (Model-I) to 0.4 mm (Model-II), the total area under damage in the bond-line (A-D) increases in the AL side (Section-I) from 17.50% in Model-I to 24.7% in Model-II, while the area under damage in the PPA side for Model-II decreased by 1.59% in comparison to Model-I (23.19%). The least difference between the peak  $\tau_{xy}/\tau_{avg}$  (as it is shown in Table 4) can explain the smaller asymmetrical behaviour of the SDEG for Model-II in bond-line (A-D).

In addition, the larger area of the overlap (E-F) with higher SDEG value is under damage for Model-II compared to other designs. However, increasing the thickness of the AL patches from 0.4 mm (Model-II) to 0.8 mm (Model-IV) decreases the total area under damage in bond-line (A-D) in the PPA side from 21.6% in Model-II to 14.4% in Model-IV with a significant drop in SDEG value.

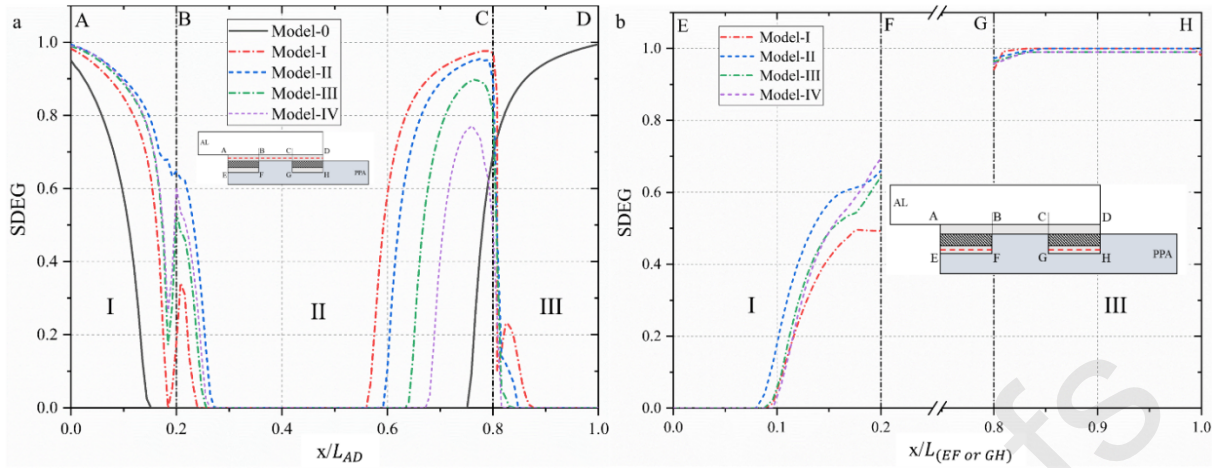


Figure 12: SDEG plot for dissimilar SLJs with different thickness of the AL patches at (a) Adhesive layer (A-D) and (b) Adhesive layer (E-F and G-H) under maximum failure load

As can be seen from Figure 13(a), by increasing the length of the AL patches, the crack initiation at the PPA side propagates at the inner section of the bond-line (A-D) without a noticeable change in the total area under damage in the bond-line (A-D). However, the total area under damage in bond-line (E-F) decreased significantly from 11.2% in Model-II to 4.8% in Model-V (Figure 13(b)). This can be explained by the significantly higher stress concentration at the bond-line (G-H) in comparison to the bond-line (E-F) for the longer AL patches. As can be seen from Figure 15, in Model-VII, the damage mostly develops in the bond-line (E-F) with only 22% of the bond-line (A-D) under damage, which is also observed experimentally.

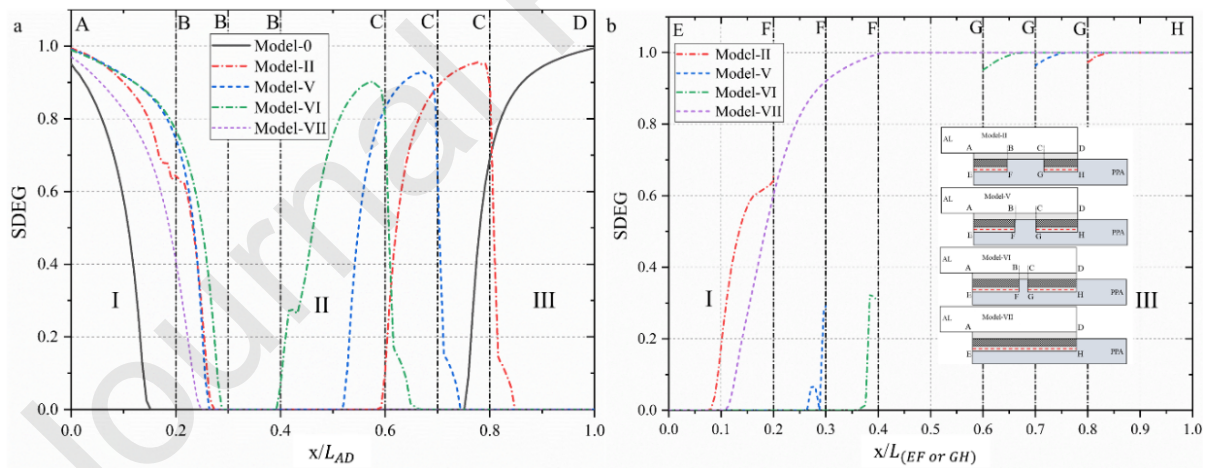


Figure 13: SDEG plot for dissimilar SLJs with different length of the AL patches at (a) Adhesive layer (A-D) and (b) Adhesive layer (E-F and G-H) under maximum failure load

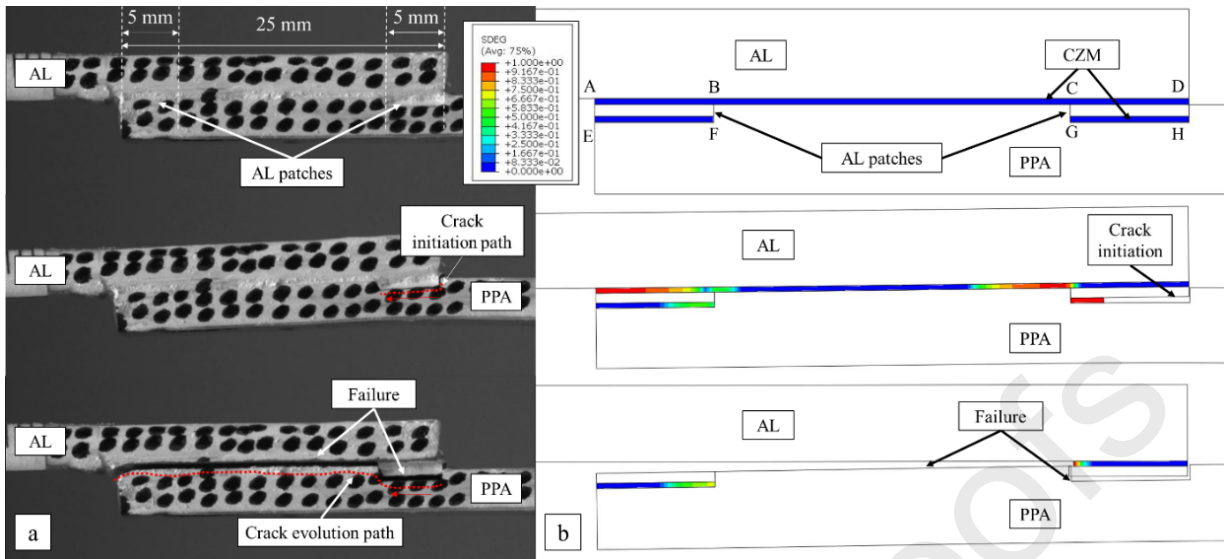


Figure 14: The (a) experimental and (b) numerical failure process of Model-II

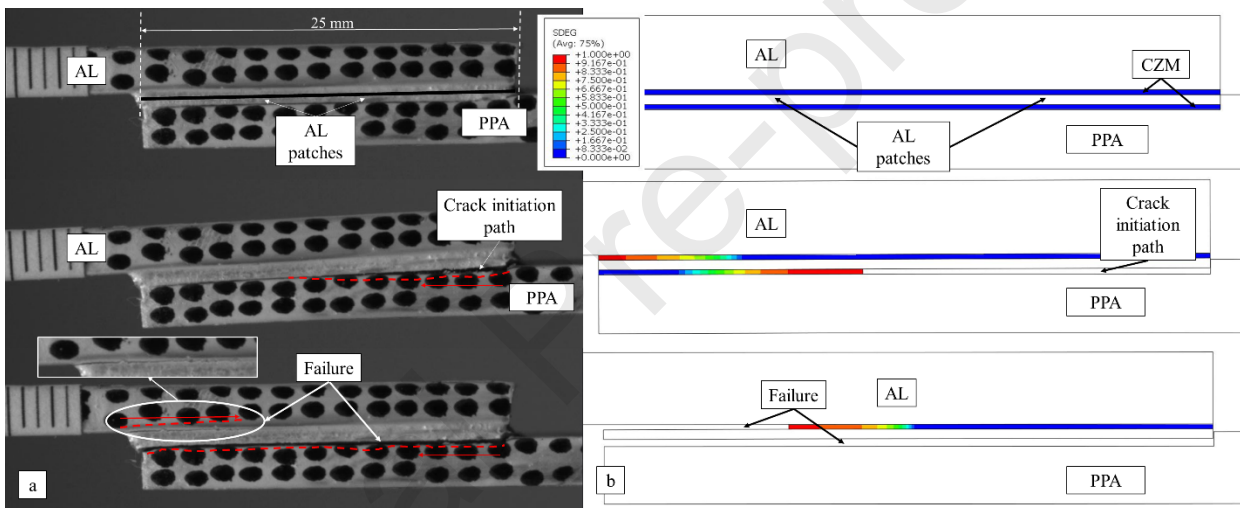


Figure 15: The (a) experimental and (b) numerical failure process of Model-VII

## 5. Conclusion

In this work, a novel design with interfacial stiffness improvement was developed to improve the strength and stress distribution of dissimilar single-lap joints. The interfacial modification was done by adding aluminium patches with different thicknesses and lengths to the interface of the lower stiffness adherend (PPA). Stress analyses using FEA was carried out to find the optimum designs based on the interfacial stress distribution. The experimental tensile tests were carried out for all modified dissimilar SLJs to find the effect of each parameter on the joints strength. Finally, the fracture process of each design was studied numerically and verified by the experimental results. The following observations have been found from the experimental and numerical results:

- The stress distribution in the dissimilar SLJ is asymmetric with higher peak value toward the lower stiffness adherend. The peak shear stress at the end of the bond-line (A-D) of the novel dissimilar SLJs (Model-I, Model-II, Model-III and Model-IV) is significantly lower than that

of the unmodified SLJ (Model-0). This is attributed to the interfacial stiffness improvement of the adherend with lower stiffness, which leads to higher global rigidity of the joint and a lower bending rotation.

- In order to take the maximum advantage of this novel configuration, it is essential to assess the effectivity of using metal patches, including length, thickness. The stress analysis shows that the AL patch with 0.4 mm thickness and 5 mm length (Model-II) has the best performance with the least difference between the shear peak stress at the edges, which results in a significant reduction in the unsymmetric shear stress distribution.
- The experimental results show that the proposed novel design provides a significant improvement in the performance of the dissimilar SLJ, which makes them significantly stronger than the conventional dissimilar SLJ design. However, increasing the thickness or length of the AL patches to achieve a higher failure load for the proposed dissimilar bonded joint is only effective within a limited range. The general trend shows that high performance could not be achieved when the ratio of the bond-line (A-D) length to the bond-line (E-F or G-H) length of the proposed dissimilar SLJ decreases. The worst performance is achieved when the ratio equals to 1. On the other hand, when the ratio of the adherend thickness to the thickness of the AL patches decreases from 15 to 7.5, the maximum failure load is improved slightly, but by decreasing the ratio furthermore to 5, the maximum failure load decreased significantly.
- The SDEG plots show that the larger area of the over-lap (A-D, E-F and G-H) is under damage in the novel design of SLJs with a smaller thickness (Model-I and Model-II) of AL patches. Increasing the length of the AL patches does not change the total area under damage noticeably in bond-line (A-D) while the smaller percentage of damage develops in bond-line (E-F and G-H) for the larger length of the AL patches.

#### **Conflict of interest**

There is no conflict of interest in this research work.

#### **Acknowledgements**

The authors wish to acknowledge the support of the Engineering Department of Lancaster University, UK.

#### **Date availability statement**

The raw/processed data required to reproduce these findings cannot be shared at this time as the data also forms part of an ongoing study.

## References:

- [1] Z. J. Wu, A. Romeijn, and J. Wardenier, "Stress expressions of single-lap adhesive joints of dissimilar adherends," *Compos. Struct.*, vol. 38, no. 1–4, pp. 273–280, May 1997.
- [2] D. Hara and G. O. Özgen, "Investigation of Weight Reduction of Automotive Body Structures with the Use of Sandwich Materials," *Transp. Res. Procedia*, vol. 14, pp. 1013–1020, Jan. 2016.
- [3] L. . Vogelesang and A. Vlot, "Development of fibre metal laminates for advanced aerospace structures," *J. Mater. Process. Technol.*, vol. 103, no. 1, pp. 1–5, Jun. 2000.
- [4] P. N. B. Reis, J. A. M. Ferreira, and F. Antunes, "Effect of adherend's rigidity on the shear strength of single lap adhesive joints," *Int. J. Adhes. Adhes.*, vol. 31, no. 4, pp. 193–201, Jun. 2011.
- [5] F. L. Matthews, P. F. Kilty, and E. W. Godwin, "A review of the strength of joints in fibre-reinforced plastics. Part 2. Adhesively bonded joints," *Composites*, vol. 13, no. 1, pp. 29–37, Jan. 1982.
- [6] X. Shang, E. A. S. Marques, J. J. M. Machado, R. J. C. Carbas, D. Jiang, and L. F. M. da Silva, "Review on techniques to improve the strength of adhesive joints with composite adherends," *Compos. Part B Eng.*, vol. 177, p. 107363, Nov. 2019.
- [7] A. Nemati Giv, M. R. Ayatollahi, S. H. Ghaffari, and L. F. M. da Silva, "Effect of reinforcements at different scales on mechanical properties of epoxy adhesives and adhesive joints: a review," *J. Adhes.*, vol. 94, no. 13, pp. 1082–1121, Nov. 2018.
- [8] T. Sawa, J. Liu, K. Nakano, and J. Tanaka, "Two-dimensional stress analysis of single-lap adhesive joints of dissimilar adherends subjected to tensile loads," *J. Adhes. Sci. Technol.*, vol. 14, no. 1, pp. 43–66, 2000.
- [9] J. R. Vinson, "Adhesive bonding of polymer composites," *Polym. Eng. Sci.*, vol. 29, no. 19, pp. 1325–1331, Oct. 1989.
- [10] A. Rudawska, "Adhesive joint strength of hybrid assemblies: Titanium sheet-composites and aluminium sheet-composites—Experimental and numerical verification," *Int. J. Adhes. Adhes.*, vol. 30, no. 7, pp. 574–582, Oct. 2010.
- [11] A. M. G. Pinto, A. G. Magalhães, R. D. S. G. Campilho, M. F. S. F. de Moura, and A. P. M. Baptista, "Single-Lap Joints of Similar and Dissimilar Adherends Bonded with an Acrylic Adhesive," *J. Adhes.*, vol. 85, no. 6, pp. 351–376, May 2009.
- [12] W. Tu, P. H. Wen, P. J. Hogg, and F. J. Guild, "Optimisation of the protrusion geometry in Comeld™ joints," *Compos. Sci. Technol.*, vol. 71, no. 6, pp. 868–876, Apr. 2011.
- [13] S. Ucsnik, M. Scheerer, S. Zaremba, and D. H. Pahr, "Experimental investigation of a novel hybrid metal–composite joining technology," *Compos. Part A Appl. Sci. Manuf.*, vol. 41, no. 3, pp. 369–374, Mar. 2010.
- [14] J. Jahn, M. Weeber, J. Bochner, and R. Steinhilper, "Assessment Strategies for Composite-metal Joining Technologies – A Review," *Procedia CIRP*, vol. 50, pp. 689–694, Jan. 2016.
- [15] M. S. Islam and L. Tong, "Influence of pinning on static strength of co-cured metal-GFRP hybrid single lap joints," *Compos. Part A Appl. Sci. Manuf.*, vol. 84, pp. 196–208, May 2016.
- [16] M. Rezvaninasab, M. Farhadinia, A. Mirzaei, M. Ramzaninezhad, F. Khamseh, and M. h. Alaei, "Experimental evaluation of reinforcing the single lap joint in both longitudinal and transverse direction under tensile and bending condition," *Int. J. Adhes. Adhes.*, vol. 88, pp. 19–25, Jan. 2019.

- [17] R. Matsuzaki, M. Shibata, and A. Todoroki, "Improving performance of GFRP/aluminum single lap joints using bolted/co-cured hybrid method," *Compos. Part A Appl. Sci. Manuf.*, vol. 39, no. 2, pp. 154–163, Feb. 2008.
- [18] R. Matsuzaki, M. Shibata, and A. Todoroki, "Reinforcing an aluminum/GFRP co-cured single lap joint using inter-adherend fiber," *Compos. Part A Appl. Sci. Manuf.*, vol. 39, no. 5, pp. 786–795, May 2008.
- [19] A. Fawcett, X. Chen, X. Huang, and C. Li, "Failure analysis of adhesively bonded GFRP/aluminum matrix single composite lap joint with cold worked penetrative reinforcements," *Compos. Part B Eng.*, vol. 161, pp. 96–106, Mar. 2019.
- [20] D. G. dos Santos, R. J. C. Carbas, E. A. S. Marques, and L. F. M. da Silva, "Reinforcement of CFRP joints with fibre metal laminates and additional adhesive layers," *Compos. Part B Eng.*, vol. 165, pp. 386–396, May 2019.
- [21] M. A. Morgado, R. J. C. Carbas, E. A. S. Marques, and L. F. M. da Silva, "Reinforcement of CFRP single lap joints using metal laminates," *Compos. Struct.*, vol. 230, p. 111492, Dec. 2019.
- [22] P. P. Camanho, C. M. L. Tavares, R. de Oliveira, A. T. Marques, and A. J. M. Ferreira, "Increasing the efficiency of composite single-shear lap joints using bonded inserts," *Compos. Part B Eng.*, vol. 36, no. 5, pp. 372–383, Jul. 2005.
- [23] A. Y. Kanani, Y. Liu, D. J. Hughes, J. Ye, and X. Hou, "Fracture mechanisms of hybrid adhesive bonded joints: effects of the stiffness of constituents," *Int. J. Adhes. Adhes.*, p. 102649, Jun. 2020.
- [24] Y. Hua, A. D. Crocombe, M. A. Wahab, and I. A. Ashcroft, "Continuum damage modelling of environmental degradation in joints bonded with EA9321 epoxy adhesive," *Int. J. Adhes. Adhes.*, vol. 28, no. 6, pp. 302–313, Sep. 2008.
- [25] R. D. S. G. Campilho, M. D. Banea, J. A. B. P. Neto, and L. F. M. da Silva, "Modelling of Single-Lap Joints Using Cohesive Zone Models: Effect of the Cohesive Parameters on the Output of the Simulations," *J. Adhes.*, vol. 88, no. 4–6, pp. 513–533, Apr. 2012.
- [26] R. D. S. G. Campilho, M. F. S. F. de Moura, and J. J. M. S. Domingues, "Modelling single and double-lap repairs on composite materials," *Compos. Sci. Technol.*, vol. 65, no. 13, pp. 1948–1958, Oct. 2005.
- [27] J. O. S. Silva, R. D. S. G. Campilho, and R. J. B. Rocha, "Crack growth analysis of adhesively-bonded stepped joints in aluminium structures," *J. Brazilian Soc. Mech. Sci. Eng.*, vol. 40, no. 11, p. 540, Nov. 2018.
- [28] B. Zhao, Z.-H. Lu, and Y.-N. Lu, "Two-dimensional analytical solution of elastic stresses for balanced single-lap joints—Variational method," *Int. J. Adhes. Adhes.*, vol. 49, pp. 115–126, Mar. 2014.
- [29] W. Jiang and P. Qiao, "An improved four-parameter model with consideration of Poisson's effect on stress analysis of adhesive joints," *Eng. Struct.*, vol. 88, pp. 203–215, Apr. 2015.
- [30] A. Y. Kanani, X. Hou, and J. Ye, "The influence of notching and mixed-adhesives at the bonding area on the strength and stress distribution of dissimilar single-lap joints," *Compos. Struct.*, vol. 241, Jun. 2020.
- [31] Y. Hua, L. Gu, and M. Trogdon, "Three-dimensional modeling of carbon/epoxy to titanium single-lap joints with variable adhesive recess length," *Int. J. Adhes. Adhes.*, vol. 38, pp. 25–30, Oct. 2012.
- [32] J. R and G. N. Naik, "Single and dual adhesive bond strength analysis of single lap joint

- between dissimilar adherends,” *Int. J. Adhes. Adhes.*, vol. 92, no. May, pp. 142–153, Jul. 2019.
- [33] J. G. Kim, I. Choi, D. G. Lee, and I. S. Seo, “Flame and silane treatments for improving the adhesive bonding characteristics of aramid/epoxy composites,” *Compos. Struct.*, vol. 93, no. 11, pp. 2696–2705, Oct. 2011.
- [34] D. S. Kwon, S. H. Yoon, and H. Y. Hwang, “Effects of residual oils on the adhesion characteristics of metal-CFRP adhesive joints,” *Compos. Struct.*, vol. 207, no. July 2018, pp. 240–254, Jan. 2019.
- [35] B. Wang, X. Hu, and P. Lu, “Improvement of adhesive bonding of grit-blasted steel substrates by using diluted resin as a primer,” *Int. J. Adhes. Adhes.*, vol. 73, no. November 2016, pp. 92–99, Mar. 2017.
- [36] Dassault Systèmes Simulia, “Abaqus CAE User’s Manual,” *Abaqus 6.12*, p. 1174, 2012.

### Author Statement

**Armin Yousefi Kanani:** Methodology, Investigation, Formal analysis, Validation, Writing - Original Draft

**Xiaohan Hou:** Conceptualization, Methodology, Supervision, Writing- Reviewing and Editing

**Jianqiao Ye:** Conceptualization, Methodology, Supervision,  
Writing- Reviewing and Editing.

Journal Pre-proofs